DESIGN COMPARISON OF LUNAR RETURN CONFIGURATIONS*

BY

E. Offenhartz, C. F. Berninger, W. Zeh, and M. C. Adams
Avco Research and Advanced Development Division, Wilmington, Mass.

Abstract

Parabolic manned re-entry design comparisons are made between two classes of slender and blunt configurations capable of conventional horizontal and vertical earth landings. Aerodynamic modulation using flaps and control augmentation requirements are discussed in terms of their effect upon re-entry trajectories and landing footprints. Within the environment defined by the re-entry trajectories, the convective and radiative modes of heat transfer are compared, their differences discussed, and the problems associated with the configurations for planetary return missions indicated. Thermal protection systems are discussed and the factors influencing the selection of a given system for the re-entry environment are indicated. Comparison between reflective and absorptive systems are made and the merits of each for a given flight time indicated. A thermo-structural analysis is presented which shows the trade-off between structural operating temperature and heat protection system thickness requirements. Total heat shield and structural weights are compared for the landing footprints presented and their variation with range shown. Finally, the areas of uncertainty in the aero-thermo structural design analysis are indicated for each class of configuration studied, and the weight differences between conventional horizontal landing and vertical descent configurations are given.

Introduction

Manned circumlunar flight and its associated re-entry phase presents new and novel problem areas. While many of these problems are within the state of the art for solution, the extrapolation of existing types of space vehicle and re-entry vehicle systems to this application requires careful consideration. The problems associated with parabolic re-entry have been treated in detail in the literature (references 1, 2, and 3). These studies indicate significant design parameters but do not enable direct comparison of configuration requirements as needed in determination of final system requirements.

In order to discuss the problems of manned re-entry and compare configurations, certain ground rules were established. A fixed internal volume of 350 ft.^{3} was assumed to be sufficient to house and support three astronauts and their associated equipment for a period of approximately two weeks. Two classes of configurations were then studied. The first were blunt configurations capable of vertical or parachute landings and the other was of the lenticular type capable of horizontal or conventional landing. All configurations considered were to have a hypersonic L/D capability of at least 0.5, considered adequate for maneuverability. Each configuration was designed to use the same basic heat protection system, structural operating temperature, and be operable for the same re-entry corridor and landing area by using a flap arrangement for modulation.

Configurations

The very blunt or high-drag configurations suitable for parachute landings and blunt, moderate-drag bodies suitable for conventional landings were studied. Figure 1 shows the outline and general dimensions of the configurations considered.

The cone had a bluntness ratio of 0.55 and a semi-vertex cone angle of 12 degrees. The calculated hypersonic lift-to-drag (L/D) capability was approximately 0.7. The center of gravity was located along the axis of symmetry and the vehicle trimmed at zero-degree angle of attack without flaps. Pitch and roll control were obtained with flaps located on the aft portion of the blunt cone. The controls operate differentially for roll control and in pairs for pitch control. At an L/D of one-half, the trim angle of attack was calculated to be approximately 19 degrees.

The 30-degree half-blunt cone configuration has a maximum calculated L/D of approximately one-half and trims without flaps at an angle of attack of approximately 4 degrees, the angle being measured from a plane parallel to the top flat surface of the vehicle. Pitch, yaw, and roll control is accomplished by four flaps; two of which extend aft from the top flat surface of the vehicle, the other two extend from the aft conic portion of the body.

The third blunt face configuration studied is shown in figure 1. An L/D of approximately one-half is calculated for this configuration which corresponds to an angle of attack of approximately

*This work was done at the AVCO Research and Advanced Development Division partially funded by subcontract NAS-5-304, GDA 203-429-A, and AVCO Corporate Funds.

35 degrees. At the trim condition the afterbody is not in the flow. Four chin flaps are used to provide pitch and yaw control.

The shapes discussed do not have capability for landing without auxiliary drag and/or lift devices, such as a parachute or a Rogallo Paraglider (reference 4). A configuration which has promise as an acceptable re-entry body with conventional glide landing capability is the lenticular shape (reference 5) where the cross section is elliptical and plan form is circular. The lenticular shape re-enters as a blunt body. After re-entry, the body is pitched to a glide position for landing. Altitude control is provided with flaps as indicated in figure 1.

Trajectory Studies

In order to determine the heating and loads associated with re-entry at parabolic velocities, trajectory studies were undertaken for flight along both the overshoot boundary at an L/D of 0 and by Chapman's 10g undershoot boundary at an L/D of 1/2. The entry corridor so bounded is approximately 30 nautical miles. Figure 2 shows a plot of altitude vs. down-range for re-entry trajectories on the over- and undershoot boundaries. The re-entry flight corridor is established by the range overlap which can be achieved for entries made on both the over- and undershoot boundaries. The maximum range shown is established by flight on the 10g lifting undershoot trajectory. Entry is made with an L/D of $\pm$ 1/2 to pull-up. When the flight path angle reaches $\pm 1.6^{\circ}$, the lift is removed and a ballistic flight is followed to an altitude of about 300,000 feet. At this altitude an L/D of $\pm$ 1/2 is again applied and held constant to impact. This maximum range can also be reached by flight on the ballistic overshoot boundary. On this boundary entry is made with L/D of 0 to impact.

The altitude of near 300,000 feet was chosen as a limiting value for skip-out, since at this altitude aerodynamic forces start to become important for control considerations.

The minimum range is obtained by entry on the ballistic overshoot boundary using a negative lift, trajectory. A modulation is made to limit the load at some point in the trajectory to 10g. This minimum range can also be achieved on the undershoot boundary by a modulation from the pull-up altitude. Ballistic flight from the bottom of the pull-up comes close to providing this range.

Due to the trajectory analysis studies, certain design restraints were established. These restraints are based upon trajectory sensitivity to flight path angle. For example, the initial ballistic overshoot re-entry angle is -5.37°. If the re-entry angle is just .02 degrees shallower or -5.35° then the resultant peak altitude after pull-up is increased by a factor of 6 from 300,000 feet to 1.8×10^{6} feet.

Furthermore, for the 10g lifting undershoot boundary a similar sensitivity exists. However, in this case, the flight path angle associated with the second (ballistic) portion of the flight is the critical parameter. For example, if the lift is removed when the flight path is 3.2° instead of 1.6° then instantaneous, full negative lift will not prevent the vehicle from skipping out.

Hence, these sensitivities to flight path angles and changes in modulation form the basic inputs required to define the guidance and control system (reference 6).

The flight corridor established by the above procedure provides an overlap in down-range of roughly 2,800 n.m. Results of investigations of the requirements of the system, the capabilities of the vehicle, and the guidance and control system indicate that this flight corridor appears to provide a reasonable approach for vehicle design criteria.

Design trajectories of this type were computed for each configuration studied in order to determine the environment which formed the basis of configuration comparison. Altitude-velocity graphs for the ballistic overshoot and 10g lifting undershoot trajectories are indicated in figure 3. The region of high convective heat flux and non-equilibrium radiation phenomena are indicated and are discussed in the re-entry heating section.

The landing capability of a vehicle with $W/C_DA = 50$ lbs./ft.^{2} which enters the atmosphere at the ballistic overshoot and 10g lifting undershoot bounds was examined. The footprint for a given re-entry angle is obtained by suitably banking the vehicle within the trajectory constraints. Once the landing footprints, associated with both entry boundaries, have been established their intersection represents the landing capability.

The maneuver capability was investigated by generating trajectories wherein the L/D and roll angle were represented as step functions. These changes were initiated at the pull-up point and at the top of the ship phase. The landing footprint obtained is indicated in figure 4. The results indicate a down-range maneuvering capability of 2,380 nautical miles and a cross-range capability of $\pm$ 420 nautical miles measured from a minimum down-range impact point which is 870 nautical miles from entry.

If the skip-out altitude requirement is relaxed, the landing footprint can be extended as indicated in figure 4. For an L/D of one-half, increasing the skip-out altitude to 500,000 feet enables the down-range capability of the vehicle to be increased by a factor of approximately 2. Care must be exercised in the choice of re-entry

trajectories and resulting landing footprints. These considerations must include the guidance and control accuracy, total heating to be absorbed as well as many other system requirements.

Re-entry Heating

The convective and diffusive stagnation point heat transfer rates were calculated using the results of Fay and Riddell (reference 7) correlated as,

$$\dot{q}_{STG} = \frac{0.76}{Pr^{0.6}} (\rho\mu)_w^{0.1} (\rho\mu)_{STAG}^{0.4} \left[1 + (Le^{0.52} - 1)\frac{h_d}{H}\right](H - h_w) \sqrt{\left(\frac{du_e}{ds}\right)_{STAG}} \sqrt{\frac{K+1}{2}} \qquad (1)$$

The factor $\sqrt{\frac{K+1}{2}}$ has been used to calculate the correction for the stagnation point velocity gradient for asymmetric configurations. "K" is defined as the ratio of velocity gradients along the principal radii of curvature (reference 8).

For a sphere, the stagnation point velocity gradient is accurately predicted by Newtonian theory. Vinokur (reference 9) evaluated constant density solutions for bodies with elliptic cross-section noses. Comparison of the data obtained for various blunt bodies (reference 10) with Vinokur's results (figure 5) indicates an over-estimation of 20 percent in the predicted velocity gradient, hence, 10 percent in heat transfer rate. In the results to be presented, Vinokur's constant density solutions were used to evaluate the stagnation point velocity gradients.

Equation 1 has been used with great success for correlating data for satellite flight velocities and altitudes less than 250,000 feet. At near escape velocities, however, the electron concentrations and temperatures in the boundary layer are large enough so as to effect transport properties of the air. The results presented in reference 11 indicate that a vehicle entering at parabolic velocity will experience approximately a 15 percent increase in stagnation point heat transfer rate over that predicted by equation 1.

These results have been compared with experimental data (reference 12) at velocities between 32,000 and 39,000 ft./sec. Within the accuracy of the data ($\pm$ 15 percent) the theory is in good agreement with the data and because the integrated electronic effect on heat transfer throughout the entire trajectory results in a smaller increase, this effect was not included in the analysis.

Heat transfer distributions require a knowledge of the pressure distributions. Wherever possible, available data applicable to the configurations studied was used. The prediction of pressure distributions for axisymmetric and/or two dimensional bodies is established in the literature. An approximate blunt body solution and the method of characteristics for equilibrium (reference 13) were employed for applicable configurations. In many cases, simple approximations, which have been found to correlate with data, were used. An approximate method used for the blunt vehicles was the technique of Lees wherein the Newtonian pressure distribution was assumed until the pressure gradient matched the gradient obtained from a Prandtl-Meyer expansion.

The convective and diffuse heat transfer distributions were calculated using the results of Kemp, Rose, and Detra (reference 14) given as:

$$\frac{\dot{q}}{\dot{q}_{STG}} = \frac{\rho_w \mu_w}{\sqrt{2\xi}} \rho_e \mu_e K \left\{2 \rho_w \mu_w \left(\frac{du_e}{ds}\right)\right\}_{ST}^{-\frac{1}{2}} \left(\frac{1 + .096\sqrt{\beta}}{1.068}\right) \qquad (2)$$

Angle-of-attack studies indicate that equation 2 can be applied to nonaxisymmetric flow by considering the flow to be pseudo-axisymmetric and evaluating the distribution along streamlines. Experimental studies (reference 15 and 16) have shown that the heat transfer distribution along meridians located at $\pm$ 90 degrees circumferentially from the windward plane of symmetry are essentially constant for moderate angles of attack. Because of angle of attack, the shift in the position of the stagnation point creates an uncertainty in heating calculations. However, comparison of Newtonian predictions with existing data resulted in empirical estimates of the stagnation point movement.

In addition to the convective and diffuse modes of heat transfer, considerations of equilibrium and non-equilibrium radiation were included in the study. For calculation of equilibrium radiation stagnation point heat transfer, Kivel's method (reference 17) was used in conjunction with shock detachment distances which were estimated using Serbin's (reference 18) and Vinokur's (reference 8) results.

Non-equilibrium Radiation *

The temperature and density gradients in the shock wave enveloping a re-entry configuration act to increase the collision frequency which results in the excitation of the vibrational, dissociative, and electronic states. The reaction rates which govern the excitations are functions of local density and temperature. The temperature, density, and concentration profiles become asymptotic to equilibrium values downstream of the shock wave.

* Reference AERL Report RR 112, "Radiation from the Non-equilibrium Shock Front," by J. D. Teare, S. Georgiev, and R. A. Allen; presented at the October 1961 ARS International Hypersonic Conference in Boston, Mass.

Both shock thickness and relaxation distance vary inversely with density. Up to altitudes where the shock thickness and the average relaxation distance are approximately equal, equilibrium conditions exist immediately behind the shock wave. At higher altitudes, where relaxation distances are much greater than the shock thickness, a temperature overshoot will occur due to the high translational temperature. At the same time, the density increases from its ideal gas value immediately behind the shock wave because dissociation increases the number of particles per unit volume. This reaction zone gives rise to the non-equilibrium radiation effects. As indicated in figure 3, non-equilibrium radiation is expected to occur in an altitude region between 150,000 and 200,000 feet at velocities greater than 30,000 ft./sec. The significance of this effect can be illustrated by the fact that for a velocity of 36,000 feet per second, and an altitude of 200,000 feet, the peak overshoot temperature is approximately four times the equilibrium temperature.

It is interesting to note that the manned lunar return flight becomes one of the first problems wherein non-equilibrium radiation phenomena may play an important design role.

To illustrate the results of the heating calculations, the stagnation point time history for the 12 degree blunted cone configuration is shown in figure 6. The convective, equilibrium, and non-equilibrium values are shown indicating that for this case, the peak radiative contribution is approximately 82 percent of the peak convective rate. The pulses associated with the radiative contribution are short in time and occur slightly earlier than the convective pulse.

The integrated stagnation point heating is shown in figure 7 wherein the integrated non-equilibrium heating is 26 percent of the convective value.

The results shown for the cone are typical of the stagnation point calculations completed for all the configurations studied. In general, the results indicate the relative order of magnitudes of heating associated in decreasing order with convective, non-equilibrium radiative, and equilibrium radiative fluxes.

In addition to the stagnation point calculations equation 2 was used to generate heating distributions and the resultant total integrated flux determined for each re-entry trajectory considered. The results of these studies indicated that the maximum heat to be absorbed by a given configuration was determined by the maximum down-range achievable by flight along the lifting undershoot trajectory. Therefore, the heat protection system was designed for this case and its performance evaluated for the other flight conditions.

Although results are not presented, heating was calculated for each of the flaps associated with a given configuration. In general, the flaps arranged along the forward blunt portion of the body were subject to stagnation point heating whereas trailing edge flaps were subject in part to separated flow as well as the oblique shock ahead of the flaps. Although the flap arrangement presents a difficult local problem, they were designed to meet maneuvering requirements. Certainly maneuvering techniques which eliminate the necessity of flap arrangements result in greater efficiency and less weight.

Thermodynamic Analysis and Materials

The two-pulse heating environment previously described requires a detailed analysis of the thermal protection system capable of dissipating the energy generated during re-entry. In general, two systems capable of achieving this end are concerned with either absorbing or radiating the energy. The absorption systems considered for ballistic missile re-entry have been the heat sink and ablation concepts. The latter system uses heat absorption with phase change and for parabolic re-entry total weight considerations indicate it is preferable to the heat sink. The difference between ablative and radiative heat protection systems is associated with the exposure time and level of aerodynamic heating. Ablative systems are generally restricted to short duration exposure because of the total mass loss. Pure radiation systems are capable of longer exposure but restricted to relatively low aerodynamic heating because of the limitation of materials capable of operating at high surface temperature. The combination of ablation and radiation in a heat protection system has certain possibilities for the two-pulse heating associated with parabolic re-entry. Detailed discussions of the merits and performance of these systems are indicated in references 19, 20, and 21.

The thermal design of a heat protection system requires knowledge of the environment and loading conditions as well as specific materials properties and desired performance. Ablation materials are available over a wide range of ablation temperatures. Epoxy-base plastics are typical of low temperature ablators restricted to an operating range between 1,200-1,700°F. These materials have low densities and thermal conductivities and are suited to satellite re-entry where their performance as pure sublimers with large transpiration contribution to the heat of ablation is desirable. Intermediate ablation temperatures between 2,800 and 3,500°F can be achieved with charring plastics which are reinforced to reduce the rate at which the char spalls during re-entry. High temperature ablators operating between 4,300 and 5,000°F vary in chemical composition and thermal properties and include such materials as nylon and quartz reinforced plastics.

Using the half-blunt cone vehicle for illustrative purposes, examination of the isotherms shown in figure 8 indicate that during the first modulation period a conventional radiation design using a refractory metal or ceramic is not feasible. The lower surface temperature on both boundaries during the second modulation indicates the feasibility of radiation design during that portion of re-entry. This then indicates the possibility of the use of a combined ablation-radiation design.

Because of the many ablation materials available, parametric studies were undertaken to determine the influence of variation in both density and thermal conductivity variations on thermal design. Furthermore, variations in design performance due to ablation temperature were also studied. For purposes of design it was assumed that the basic structural member was a honeycomb structure. As will be shown later, the material used in the honeycomb structure influences the thermal history of the structural members used for longitudinal and circumferential support but does not directly influence the heat shield selection or thickness evaluation. Therefore, evaluation was made using a honeycomb structure backed by a semi-infinite thickness of a typical low strength, low density fibrous glass insulation designed to limit the temperature rise at the vehicle interior to approximately 70°F. The ablation material was an epoxy based reinforced resin capable of operation at 5,000°F. With these ground rules the results of the thermodynamic design are indicated in figure 9. The figure indicates the ablator thickness required to restrict the honeycomb structure temperature to the prescribed values. From a thermal point of view, the advantage of allowing the structure to attain a high operating temperature is obvious. The required thickness of ablation material increases with increasing aerodynamic heat input and decreasing structural operating temperature.

Structural Considerations

Preliminary structural designs and analysis were conducted to determine the relative structural advantages of each configuration. Variation of maximum operating structure temperature and the associated structural material selection was introduced as the only other significant parameter which was independent of vehicle shape.

Structural integrity was provided, in all cases, by a metallic structure behind the ablator which was designed to withstand all loading conditions without consideration of the load-carrying capability of the ablator. Each vehicle structure was designed for both 14.7 and zero psia internal pressure during re-entry. Honeycomb sandwich, reinforced with frames and longerons as required, was selected as the basic type construction. The high rigidity to flexure of this type design provides for structural stability and minimizes deflections between frames and longerons and the associated bending stresses induced in the ablator.

The use of aluminum, titanium, stainless steel, and René 41 were each considered as structure behind the ablator. The required honeycomb sandwich design and weight was computed for the blunt face vehicle for each material using load and temperature data corresponding to the worst design condition in a 10g lifting undershoot trajectory of 2,800 miles down-range distance. The unit weight of structure and heat shield are shown plotted in figure 10. Structural design comparisons of other large areas of the reference vehicles indicated a similar result. It should be mentioned that in certain cases -- particularly using steel and René -- minimum available sheet gages became a governing factor and structural weight was not directly related to operating temperatures. Figure 10 illustrates that appreciable over-all weight saving are possible by operating structure at higher limits, i.e., the savings in ablation material required for insulation more than offset increased structural weights over the temperature range considered. The maximum temperature that may be used in a practical design depends greatly on the maintenance of the heat shield-substructure bond or attachment integrity. This depends upon a number of factors such as detail design and the criteria for maintaining the heat shield on the vehicle and over-all system reliability.

A complete structural analysis is beyond the scope of this paper, however, a few comments on the differences and similarities of the design problems between vehicle shapes and the use of different structural materials is in order.

The half-blunted cone and lenticular shapes required substantial frames to resist the bending moments due to internal pressurization. Difficulty was experienced with thermal gradients and yielding within the frames for the higher temperature structural designs and tension-tie members across the vehicle compartment were used to reduce bending moments and frame depth requirements in order to avoid excessive thermal stresses. This problem was due primarily to the shapes and the internal pressure loads. The full-cone and blunt face type body with the non-symmetric aerodynamic loading did not present a comparable design problem.

Landing impact attenuation with crushable material behind the structure was also considered. Here blunt cone and half-blunt cone have an advantage over the other configurations since in the former the point of impact, on the vehicle, under different vehicle attitudes occurs over a smaller area thus permitting more efficient usage of a limited amount of crushable material and smaller internal volume used for this purpose.

The launch arrangement and tie-down systems studied showed substantial advantages for the axial symmetric bodies (blunt cone and blunt face type vehicles). The half cone and lenticular shapes resulted in more complex and generally heavier booster transition section. The lenticular shape entails considerable complexity for abort requirements and escape pods were considered necessary.

The choice of the structural material had little significance on the nature of the design problems. The membrane stresses in the composite shall (structure and ablator) distribute themselves in the ratio of their modulii; $\sigma_{abl}/E_{abl} = \sigma_{str}/E_{str}$. Since the structural materials considered have approximately the same strength-modulus ratios, each metal may be utilized at approximately the same percentage of its allowable stress for a given maximum ablator stress. The structural materials considered also have approximately the same modulus-weight ratios, and strength-weight ratios, and, since each was designed to the same loading conditions, the rigidities of the sandwich structures were comparable. The lighter materials having lower modulii and strengths had correspondingly thicker sandwich face sheets.

To explain the nature of the re-entry thermal stresses, consider the typical stresses in the ablator shown in figure 11 which corresponds to a "full restraint" such as would occur with a rigid substructure. It can be seen that the internal force ($\int \sigma dy$) occurs primarily due to stresses over a small layer of material (labeled A) which corresponds to temperatures over a range where $E\lambda\Delta T$ is appreciable, where E(T) is Young's Modulus, λ (T) is the thermal coefficient of expansion, and ΔT the temperature rise from the zero stress temperature. Small stresses exist in the outer region B due to the low modulus of the degraded (char) material. Small stresses exist in the inner region C due to the low expansion term $\lambda\Delta T$ in this "cool" region.

The thermal stress behavior for different ablator thicknesses is further illustrated by the stress-time curves shown in figures 12, 13, and 14 which are obtained from a shell solution including the effects of a steel substructure. It will be noted that the stresses on the outer surface (O.D.), mid-point, and inner surface (I.D.) of the ablator all peak at about the same value* (approximately $E\lambda\Delta T$). The peak ablator stresses for different thicknesses (vehicle locations) are all approximately of the same magnitude, although occurring at different times. Qualitatively, the peak of figure 11 "travels through" the ablator and decreases slightly in magnitude as the "restraint of the ablator" decreases with increased penetration of the degraded plastic layer.

*The effects of external pressure cause the peak stresses to be slightly greater than that of figure 11.

It is necessary to consider the relative thermal coefficients of expansions of the structures and ablators. The values given below

	$\lambda (10^{-6}/^{\circ}F)$ @ $200^{\circ}F$
Aluminum	12.9
Titanium	5
Steel	7
Ablator	61

indicate small differences between the structural materials compared to the difference between the structure and ablator. This, together with the comparable structural rigidities already discussed, explains why the nature of the thermal stress problems in re-entry were fundamentally the same for all the structures.

The contact pressure or bond stresses are shown in each case to be small. The contact pressure due to thermal stresses is, however, dependent on the radii of curvatures of the shell and therefore vehicle shape dependent. Estimates of contact pressures can be made by taking ratios of radii of curvatures. Contact stresses 10 to 20 times the values shown were found in the study but even these values do not appear to create design difficulties.

Weight Comparisons

The results of the aerothermodynamic and structural analysis can be summarized in terms of weight. The weight of the heat shield and structure for each of the vehicles studied are shown in Table I, based upon the use of a $1,000^{\circ}F$ René structure and charring ablator.

Within the accuracy of the design analysis, the weights of all blunt bodies capable of conventional parachute landing are the same. It was not possible to determine an obvious advantage between configurations based upon the assumption of a fixed internal volume and identical heat shield and structural operating temperature. Other total system requirements may determine an optimum configuration for the total mission which was not possible from the present analysis.

The weight penalty associated with the lenticular configuration capable of conventional landing is clearly indicated. It was found that a lenticular configuration having a 350 cubic foot volume could not develop sufficient subsonic L/D for landing. Therefore, a 16 foot diameter configuration was studied and the penalty shown.

The relative increase in heat shield weight is a function of down-range distance is shown in figure 15. Also shown as a design parameter are lines of constant deceleration from 4 g's to 10 g's. Confining attention to the 6 g curve, it is apparent that increasing down-range generally produces a heat shield weight penalty up to a range of 13,000 miles. This corresponds to a skip-out altitude

of approximately 750,000 feet. This results from the fact that increasing the range tends to increase the time for heat penetration into the structure and the time for radiation heat loss from the vehicle surface. Beyond this range, the radiation loss exceeds the heat diffusion effect and the weight requirement decreases. It is also apparent that for constant range, increasing the deceleration decreases the relative heat shield weight. Consequently to reduce heat shield weight, the trajectory would be restricted to shorter ranges or greater deceleration levels.

Conclusions

Blunt bodies capable of vertical descent when compared on a fixed volume basis offer little difference in terms of structural and heat protection system weight. The lenticular or conventional landing configurations studied require greater volume than blunt configuration and hence show a weight disadvantage by comparison. For vertical descent vehicles, the choice of configuration may be largely dictated by total system considerations, such as abort requirements, booster interface design, and rendezvous and docking with other vehicles in space.

Acknowledgment

The authors wish to acknowledge the contributions of Messrs. P. T. Andrews, J. A. Collins, and G. J. Cloutier to the details of the analysis presented.

References

1. Chapman, D. R., "An Analysis of the Corridor and Guidance Requirements for Supercircular Entry into Planetary Atmospheres," NASA TR R-55, 1959.

2 Grant, F. C., "Modulated Entry," NASA TN D-452, August 1960.

3. Wong, T. J., Goodwin, G., and Slye, R. E., "Motion and Heating During Atmosphere Reentry of Space Vehicles," NASA TN D-334, September 1960.

4. Rogallo, F. M., Lowry, J. G., Croom, D. R., and Taylor, R. T., "Preliminary Investigation of a Paraglider," NASA TN D-443, August 1960.

5. Jackson, C. M. and Harris, R. V., "Static Longitudinal Stability and Control Characteristics at a Mach Number of 1.99 of a Lenticular-Shaped Reentry Vehicle," NASA TN D-514, October 1960.

6. Dow, P. C., Fields, D. P., and Scammell, F. H., "Automatic Re-entry Guidance at Escape Velocity," ARS No. 1946-61, 1961.

7. Fay, J. A. and Riddell, F. R., "Theory of Stagnation Point Heat Transfer in Dissociated Air," JA/SS, February 1958.

8. Reshotko, E., "Heat Transfer to a General Three-Dimensional Stagnation Point," Jet Propulsion, January 1958.

9. Vinokur, M., "Inviscid Hypersonic Flow Near the Stagnation Point of Oblate Ellipsoidal Noses," JA/SS, July 1958.

10. Boison, J. C. and Curtiss, H. A., "An Experimental Investigation of Blunt Body Stagnation Point Velocity Gradient," ARS Journal, February 1959.

11. Adams, M. C., "A Look at the Heat Transfer Problem at Super Satellite Speeds," ARS No. 1556-60, December 1960.

12. Offenhartz, E., Weisblatt, H., and Flagg, R. F., "Stagnation Point Heat Transfer Measurements at Super Satellite Speeds," Journal of the Royal Aeronautical Society, January 1962.

13. Wood, A. D., "Machine Programming for Method of Characteristics Computation (In Vicinity of Flare Shock)," Avco RAD Technical Release 59-22, February 1959.

14. Kemp, N. H., Rose, P. H., and Detra, R. W., "Laminar Heat Transfer Around Blunt Bodies in Dissociated Air," JAA/SS, July1959.

15. Weisblatt, H., "Experimental Determination of the Laminar Heat Transfer Rate Distribution Along a Slender Blunt-Nose Body from Shock Tube Tests," Avco RAD-7-TM-60-34, June 1960.

16. Weisblatt, H., "Effect of 15° Angle of Attack on Laminar Heat Transfer Rate Distribution of a Slender Blunt-Nosed Cone-Cylinder Model," Avco RAD Technical Release 60-8, January 1960.

17. Kivel, B., "Radiation from Hot Air and Its Effect on Stagnation Point Heating," JA/SS, February 1961.

18. Serbin, H., "The High-Speed Flow of Gas Around Blunt Bodies," Aeronautical Quarterly, pp 313, 1958.

19. Collins, J. A. and Moodie, D., "Thermal Insulation for Lifting Re-entry Vehicles," ARS No. 1684-61, 1961.

20. Collins, J. A., Toscano, C., Moodie, D., and Wolz, W., "Transient Behavior of Composite Thermal Protection Systems," ARS No. 1695-61, 1961.

21. Roberts, L., "Radiation and Ablation Cooling for Manned Re-entry Vehicles," presented at the Second International Congress, International Council of the Aeronautical Sciences, Zurich, Switzerland, September 1960.

Table 1

Configuration	Heat Shield & Structure (lbs.)
Half-Blunt Cone	2,054
Blunt Cone	2,187
Blunt Body	2,136
Lenticular (16'D)	3,570

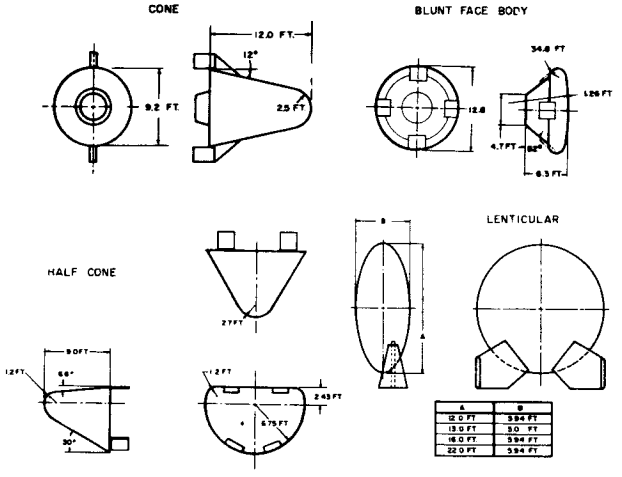

FIG 1 LUNAR RETURN CONFIGURATIONS

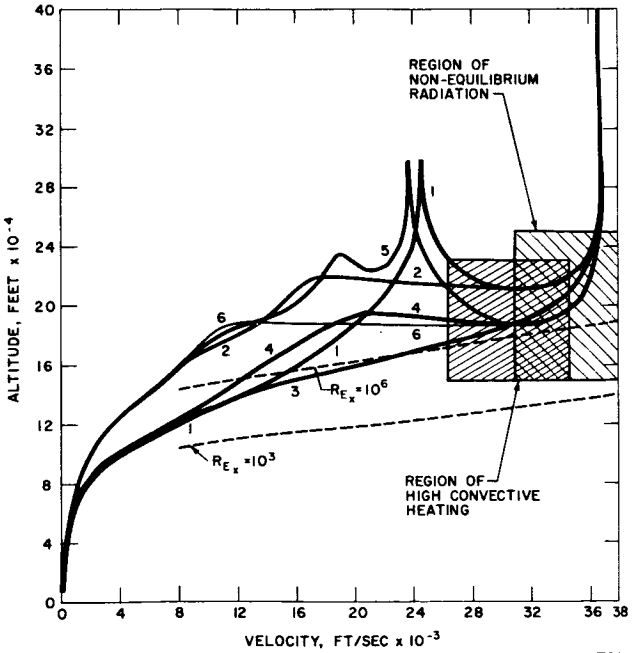

FIG. 3 ALTITUDE-VELOCITY PROFILES FOR PARABOLIC RE-ENTRY TRAJECTORIES

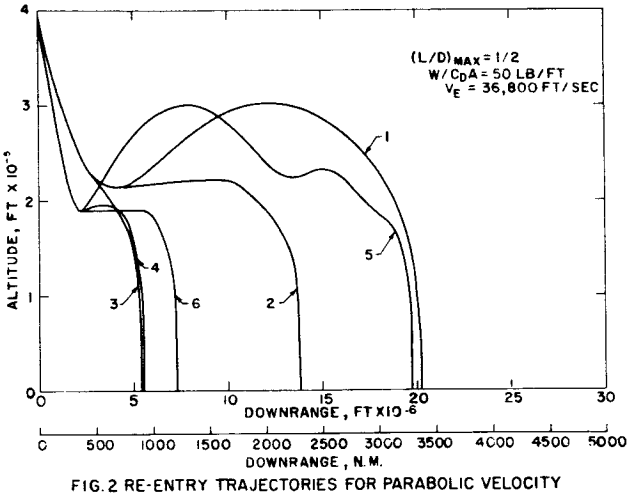

FIG. 2 RE-ENTRY TRAJECTORIES FOR PARABOLIC VELOCITY

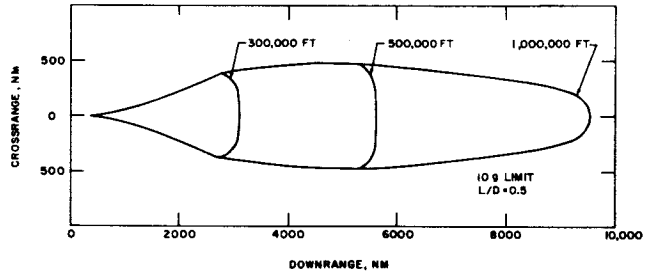

FIG.4 LANDING FOOTPRINT AS A FUNCTION OF SKIP-OUT ALTITUDE

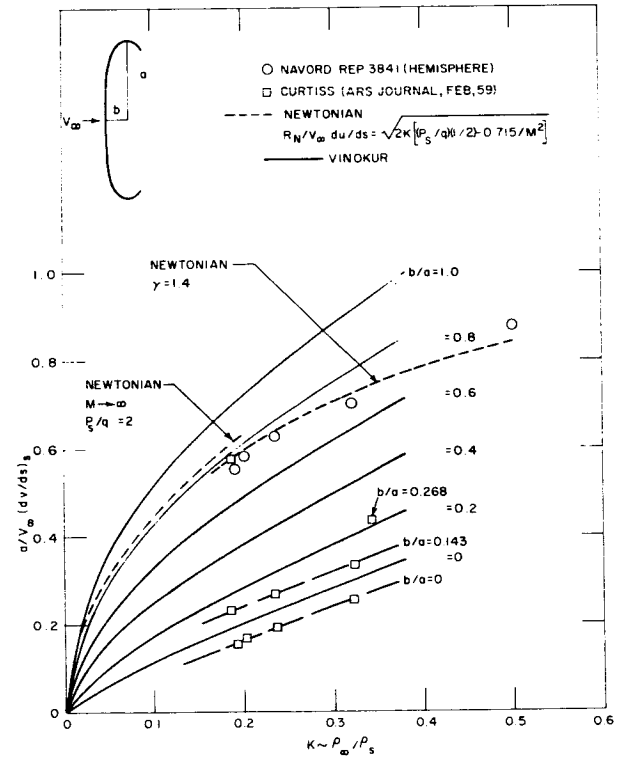

FIG.5 COMPARISON OF VINOKUR RESULTS WITH EXPERIMENTAL DATA AND NEWTONIAN THEORY

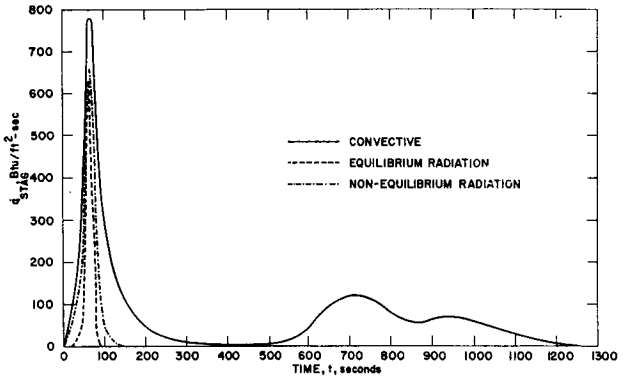

FIG. 6 STAGNATION POINT HEATING–CONE
10 G LIFTING UNDERSHOOT BOUNDARY TO MAXIMUM RANGE

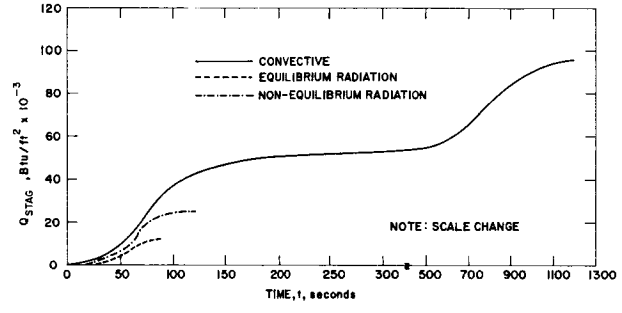

FIG. 7 INTEGRATED STAGNATION POINT HEATING–CONE
10 G LIFTING UNDERSHOOT BOUNDARY TO MAXIMUM RANGE

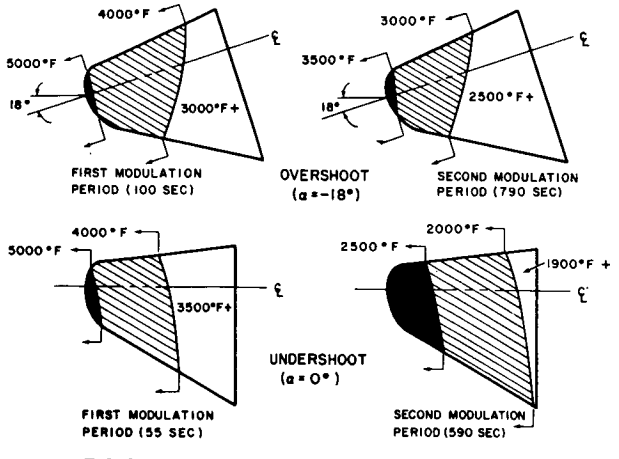

FIG. 8 MAXIMUM SURFACE TEMPERATURE FOR THE BLUNT HALF CONE

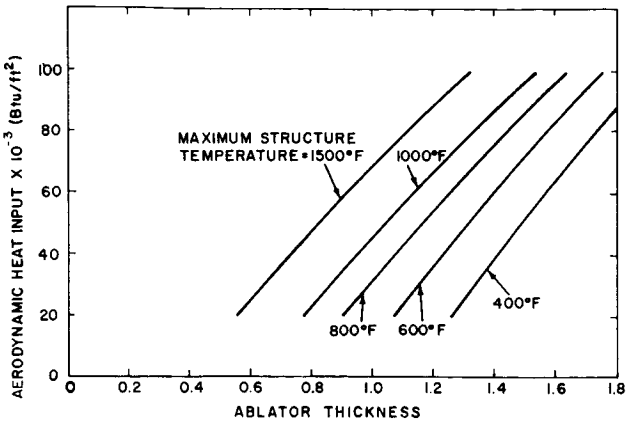

FIG. 9 THICKNESS REQUIREMENTS FOR VARIOUS STRUCTURAL OPERATING TEMPERATURES

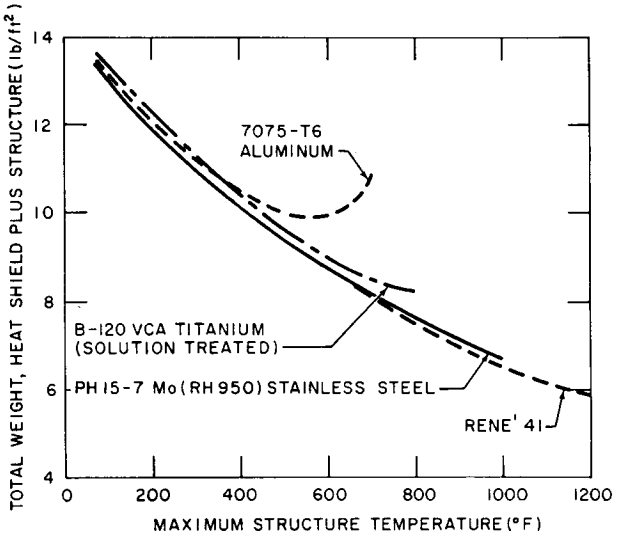

FIG. 10 COMBINED WEIGHT, HEAT SHIELD PLUS STRUCTURE BLUNT FACE VEHICLE

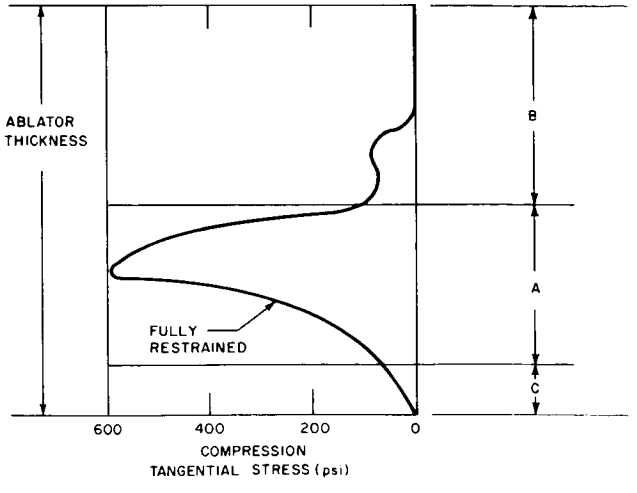

FIG. 11 STRESS DISTRIBUTION THROUGH ABLATOR THICKNESS

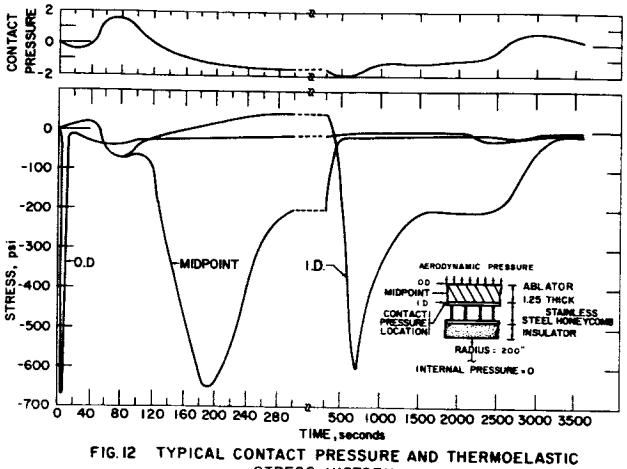

FIG. 12 TYPICAL CONTACT PRESSURE AND THERMOELASTIC STRESS HISTORY

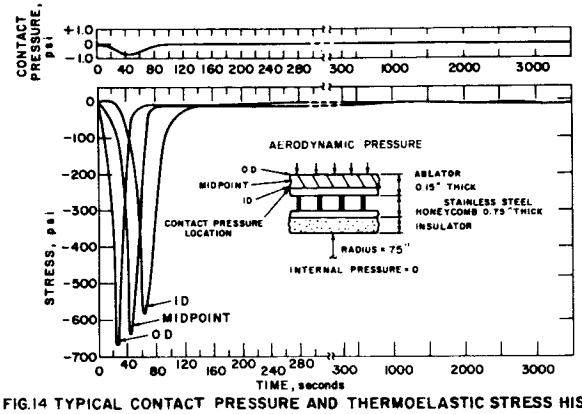

FIG. 14 TYPICAL CONTACT PRESSURE AND THERMOELASTIC STRESS HISTORY

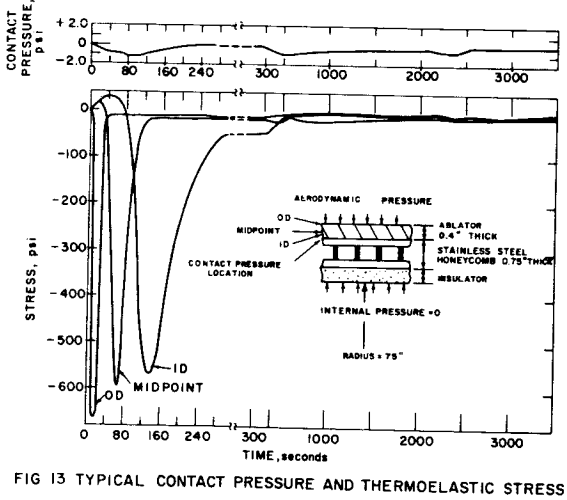

FIG 13 TYPICAL CONTACT PRESSURE AND THERMOELASTIC STRESS HISTORY

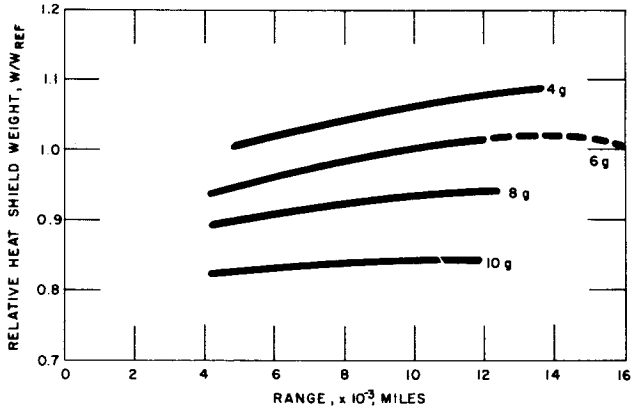

FIG. 15 INFLUENCE OF DOWNRANGE DISTANCE AND DECELERATION ON RELATIVE HEAT SHIELD WEIGHT